Article

Structural, Optical, and Renewable Energy-Assisted Photocatalytic Dye Degradation Studies of ZnO, CuZnO, and CoZnO Nanostructures for Wastewater Treatment

Awais Khalid [1,*] , Pervaiz Ahmad [2] , Roomia Memon [3], Lamyaa F. Gado [4], Mayeen Uddin Khandaker [5,6,*] , Hanadi A. Almukhlifi [7], Yosra Modafer [8], Najma Bashir [9], Otman Abida [10] , Fahdah Ayed Alshammari [11] and Abdelmajid Timoumi [12,*]

[1] Department of Physics, Hazara University Mansehra, Kandash 21300, Khyber Pakhtunkhwa, Pakistan
[2] Department of Physics, University of Azad Jammu and Kashmir, Muzaffarabad 13100, Pakistan
[3] National Centre of Excellence in Analytical Chemistry, University of Sindh, Jamshoro 76080, Pakistan
[4] National Institute of Oceanography and Fisheries (NIOF), Cairo 11516, Egypt
[5] Center for Applied Physics and Radiation Technologies, School of Engineering and Technology, Sunway University, Bandar Sunway 47500, Selangor, Malaysia
[6] Department of General Educational Development, Faculty of Science and Information Technology, Daffodil International University, DIU Rd, Dhaka 1341, Bangladesh
[7] Department of Chemistry, Faculty of Science, University of Tabuk, Tabuk 71491, Saudi Arabia
[8] Department of Biology, College of Science, Jazan University, Jazan 45142, Saudi Arabia
[9] Department of Physics, The University of Punjab, Lahore 54590, Pakistan
[10] African Sustainable Agriculture Research Institute (ASARI), Mohammed VI Polytechnic University (UM6P), Laayoune 43150, Morocco
[11] Department of Biology, Faculty of Science and Arts-RAFHA, Northern Border University, Al Arar 91431, Saudi Arabia
[12] Physics Department, Faculty of Applied Science, Umm AL-Qura University, P.O. Box 715, Makkah 12231, Saudi Arabia
* Correspondence: awais.phy@hu.edu.pk (A.K.); mayeenk@sunway.edu.my (M.U.K.); aotemoume@uqu.edu.sa (A.T.)

Abstract: Renewable energy can be harnessed from wastewater, whether from municipalities or industries, but this potential is often ignored. The world generates over 900 km^3 of wastewater annually, which is typically treated through energy-consuming processes, despite its potential for energy production. Environmental pollution is a most important and serious issue for all and their adulterations to the aquatic system are very toxic in very low concentrations. Photocatalysis is a prominent approach to eliminating risky elements from the environment. The present study developed Zinc oxide (ZnO), Copper-doped Zinc oxide (CuZnO), and Cobalt-doped Zinc oxide (CoZnO) nanostructures (NSs) by facile hydrothermal route. The crystalline and structural stability of the synthesized nanostructures were evident from XRD and FESEM analysis. Metal, and oxygen bond and their interaction on the surfaces and their valency were explored from XPS spectra. Optical orientations and electron movements were revealed from UV-Visible analysis. After 100 min exposure time with 1 g of catalyst concentration 60%, 70%, and 89% of dye degraded, for dye concentration (5 mg/L to 50 mg/L), the huge variation observed (70% to 22%), (80% to 16%), (94% to 10%). The highest photodegradation rate (55%, 75%, 90%) was observed on pH~12 using ZnO, CoZnO, and CuZnO respectively. Photodegradation of methylene blue confirmed the largest surface area, rate of recombination, photo-excited charge carriers, photo-sensitivity range, and radical generations of ZnO, CuZnO, and CoZnO. The present study, therefore, suggested that CuZnO would be preferred to produce nanomaterials for industrial wastewater treatment like methylene.

Keywords: cobalt; copper; metal doped; photodegradation; wastewater treatment; zinc oxide nanostructures

1. Introduction

In a few decades, the utilization of oxides of transition metals as a catalyst for photodegradation has increased when transition metals are doped into oxides the crystal defect is increased, and the optical band is modified because of this change in absorbance to a longer wavelength. However, among several semiconductors photocatalysts, zinc oxide (ZnO) has been employed extensively for the breakdown of organic contaminants. Because at room temperature ZnO has a wide direct band gap of 3.37 eV and has a substantial exciton binding energy in the 60 MeV range. Therefore, ZnO nanoparticles (NPs) gained a lot of attention and have a broad range of applications. In the last ten years, several reports have discussed the potential use of ZnO nanostructures (NSs) with a variety of morphologies, i.e., nanoparticles (NPs), nanoflowers, nanoballs, and nanorods, for the photocatalytic degradation of organic pollutants. To provide a few examples from the literature, Kumaresan et al. reported a modest fluctuation in the optical band gap of ZnO as a function of particle size [1]. This may be accomplished by modifying the different synthesis procedures with different morphologies and sizes, including chemical vapor deposition ablation, sol-gel method polyol process, microemulsion techniques, and hydrothermal techniques. Furthermore, the hydrothermal technique makes it possible to generate ZnO nanoparticles that have narrowed size distribution, high crystalline quality, and a controlled morphology. This approach acts as a surfactant, and stabilizing agent, and prevents the NPs from agglomerating because of the aggregation of the NPs. Many researchers have focused on developing heterojunctions of ZnO with other semiconductors having narrow bandgaps [2]. One method to reduce the limitations, and improve catalytic capabilities is to dope metal ions into ZnO photocatalysts. Because of this modification, the photocatalytic efficiency of ZnO will be enhanced and resulting in the photo-generated electron-hole pairs separation and the improvement of ZnO's ability to absorb visible light. Therefore, several different techniques for the treatment of industrial wastewater have been applied to the process of degrading organic dyes. When looking at available options, photocatalysis stands out as the most eco-friendly method since it consumes sustainable, renewable solar energy and operates at ambient temperature and pressure [3,4]. In recent years, semiconductor photocatalysts including BN [5] ZnO [6], TiO_2 [7], and Ag_2O [8] have seen widespread use in the treatment of wastewater. The CuZnO nanorods have a superior photocatalytic ability for the breakdown of diuron under UV light. Due to their unique structure, homogeneous shape, composition, and photocatalytic ability, CuZnO NPs are anticipated to bring fresh insights into a variety of applications, including solar cells and wastewater treatment. According to Awais et al. [9] research, hydrothermally produced ZnO and CuZnO-NPs were studied to determine their photocatalytic degradation capabilities for the removal of dye contaminants. Degradation of the MB dye was observed to be related to irradiation duration, with 2 h exposure to a UV source 94% of MB dye was destroyed. Dye degradation is also inversely proportional to MB dye concentration, decreasing from 94% to 20% as MB concentration is increased from 5% to 80%. Co is a highly desired and most efficient transition metal dopant for adjusting the electrical and optical properties of ZnO [10]. Lu et al. [11] used a simple hydrothermal technique to photo-catalytically active CoZnO nanorods that can destroy alizarin red dye up to 93% within 1 h. The insertion of Co not only improved charge separation and transfer capacity but also successfully blocked the recombination of photo-generated charge carriers in ZnO, leading to a high photodegradation. Sini Kuriakos et al. [12] found that nanodisks and nanorods of CoZnO have far higher photodegradation than pure ones. The increased surface area and charge separation efficiency of ZnO nanodisks due to optimum Co doping limit photogenerated charge carrier recombination, resulting in enhanced photodegradation. CoZnO nanostructures may boost photocatalytic activity. Goswami et al. [13] claimed that the synthesis approach used in this work is successful in replacing Co^{2+} ions in the ZnO lattice and generating the most efficient photocatalyst for the breakdown of organic contaminants for wastewater purification.

In the current work, ZnO, CuZnO, and CoZnO NSs were synthesized using a hydrothermal technique that is both efficient and inexpensive. MB was used to evaluate the photodegradation activity of the produced ZnO, CuZnO, and CoZnO NSs. Other factors that influence photodegradation efficiency were also evaluated. These included catalyst concentration, initial hydrogen potential (pH), and dye concentration. The synthesized photocatalyst will be used as wastewater treatment materials.

2. Materials and Methods

2.1. Materials

Cobalt-III chloride hexahydrate ($CoCl_3 \cdot 6H_2O$), Zinc chloride ($ZnCl_2$), Copper chloride dihydrate ($CuCl_2 \cdot 2H_2O$), Potassium hydroxide (KOH), and Methylene blue (MB) were purchased from Sigma-Aldrich.

2.2. Synthesis of ZnO, CuZnO, and CoZnO Nanostructures

Highly crystalline ZnO, CuZnO, and CoZnO-NSs have been synthesized by using $CoCl_3 \cdot 6H_2O$, $CuCl_2 \cdot 2H_2O$, $ZnCl_2$, and KOH as precursors. Initially, 1.6 g of $ZnCl_2$ and 0.8 g of KOH are combined in 40 mL of deionized water separately under continuous stirring at room temperature for pure ZnO. For doping Cu and Co in ZnO; $CoCl_3 \cdot 6H_2O$ and $CuCl_2 \cdot 2H_2O$ was added to get a ratio of 1:4 for each sample. Afterward, a dropwise addition of KOH solution was made to get a precipitate. As a result, the solution was agitated for 30 min at room temperature before being maintained at 150 °C for 18 h. The precipitate was first washed with double-distilled water, followed by ethanol, and then dried for 30 min at 80 °C. The whole process is demonstrated as a schematic illustration in Figure 1.
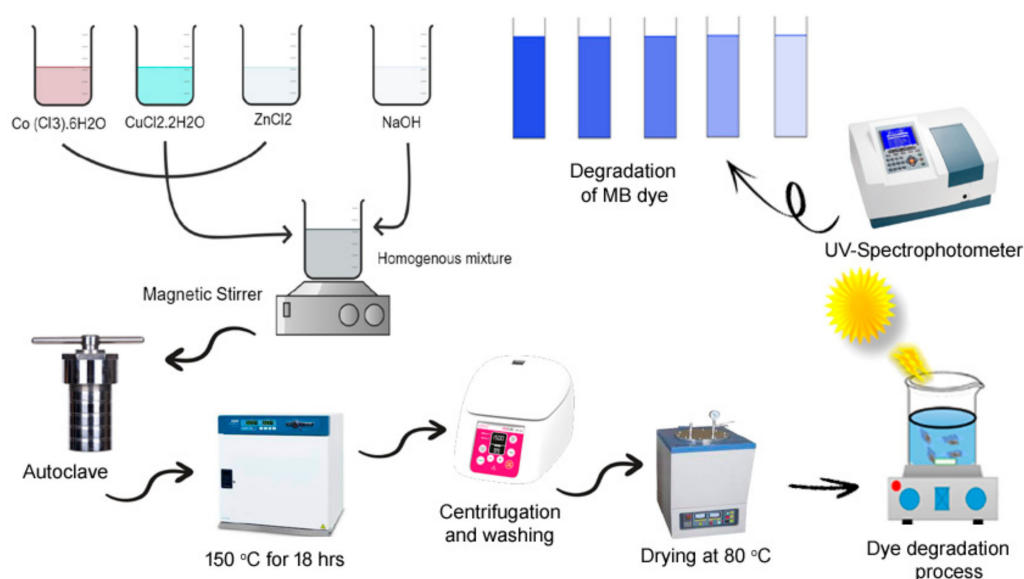
Figure 1. Schematic illustration for the complete process (synthesis to dye degradation).

2.3. Photodegradation Procedure

The photodegradation efficiency of the synthesized photocatalyst was observed using a double UV-visible spectrophotometer (model Shimadzu UV-1700). In the typical process, 0.8 g of each photocatalyst was used in a 5 mg/mL MB dye concentration. The solution was exposed to UV light while placed on a magnetic stirrer for 15 min in dark before degradation analysis. Furthermore, a 400 W tungsten lamp was used as a light source with a distance of 20 cm. To analyze the efficiency of a photocatalyst after its exposure to UV light, the solution was collected every 20 min interval. To test the recyclability of the photocatalyst, centrifugation was performed to separate the photocatalyst from the MB solution.

3. Results and Discussion

3.1. FESEM Analysis

Figure 2a–f shows the FE-SEM micrographs of the synthesized ZnO, and its nanostructure derivatives CuZnO and CoZnO. The results revealed the morphology, size, and shape of ZnO at low (10,000×) and high (20,000×) magnification, the images appear to be nanosheet-like morphology as shown in Figure 2a,b respectively. On the other hand, after the trimming process due to the addition of metal salt solution like Cu or Co ions as precursors, CuZnO and CoZnO structures were obtained. In the case of Cu ions, it is found that the bulk particles converted to very small discrete particles at the bottom that are adjacent to each other and look like cotton with gray color as seen in Figure 2c at (10,000×) magnifications, while in Figure 2d at (20,000×) magnification, it shows larger size white particles at the top of the image. It consists of agglomerated small particles; this may be due to the synthesized bulk ZnO that formed at the beginning of reactions which can degrade by the catalytic reaction using Cu ions to a nanosized range. Then these nanoparticles may agglomerate into large particles due to the inability of the KOH components as a capping agent. In this regard, when Co ions are used as precursors instead of the Cu ions, they have a higher ability for the degradation of the ZnO bulk than that observed in the case of the Cu ions. It gives a discrete or individual cuboid shape structure in a random configuration as shown in Figure 2e at the lower magnification (5000×). Figure 2f shows the higher magnification FE-SEM micrograph of CoZnO at (10,000×), it is observed clearly, the larger size crystals as well as the smaller cuboid nanocrystals. These results refer to the growth and doping process which starts with smaller particles, then develops into smaller cuboid shape structures which complete their growth during the reaction until the end of the experimental time of 18 h. These results revealed that the growth and condensation of the CoZnO continued for a duration of time. Moreover, in comparison between the synthesized ZnO derivatives structure, it is observed that the particle size of CuZnO is smaller than CoZnO, thus it is concluded that the degradation or trimming process of the ZnO bulk depends on the type of the metal ion used for trimming and the growth duration time, i.e., the obtained particles size can be controlled by these factors.

3.2. X-ray Diffraction Analysis

The structure, phase, and crystallite size of the synthesized material are analyzed using XRD. It is an analytical technique used to determine the size and nature of the material. It depends on the position and intensities of the appeared peaks. The XRD patterns of ZnO, CuZnO, and CoZnO are displayed in Figure 3. Each diffraction peak's miller indices have been calculated, and they support the synthesis of CuZnO and CoZnO in the sample. Miller indices values of each diffraction peak of CoZnO appear at 31.73, 34.63, 36.20, 47.48, 56.56, 62.79, 66.33, 67.89, and 69.05. The diffraction pattern of the sample was compared with the reference database from the "inorganic crystal structure database" (ICSD), card/file no. 01-076-0704, and crystalline phases were recognized using X'Pert High Score. Additionally, the sample showed low-intensity peaks, which are connected to the presence of Co-based oxides (Co_2O_3 and CoO). In addition, Co_2O_3 has an antiferromagnetic nature, leading to an increasing Co atomic percentage and samples' magnetization. Cobalt (II) oxide, often known as CoO, exists in two stable phases: hexagonal wurtzite and cubic rock salt. Given that CoO may also form hexagonal crystals and that Co^{2+} and Zn^{2+} have ionic radii of 0.745 and 0.74, respectively, changes in size and doping should not significantly affect the lattice parameters. An increase in Co content in ZnO causes a change in parameters [14,15]. In this respect, this figure also exhibits, the XRD pattern containing peaks of CuZnO which appear at 31.97°, 36.44°, 39.71°, 50.07°, 53.59°, 56.77, 61.71°, 66.54°, 68.08 and 69.29° corresponds to hexagonal wurtzite ZnO and CuZnO respectively (ICSD card No. 89–7102) [16,17]. Additional peaks in the XRD pattern can be found at 30.9, 38.8, 44.5, 50.2, and 53.5. Cu (II) oxide is represented by the peaks at 30.9, 38.8, and 53.5, whereas the peaks at 44.5 and 50.2 are attributed to the FCC phase of copper [18]. Cu doping in ZnO is shown by the presence of Cu and CuO.
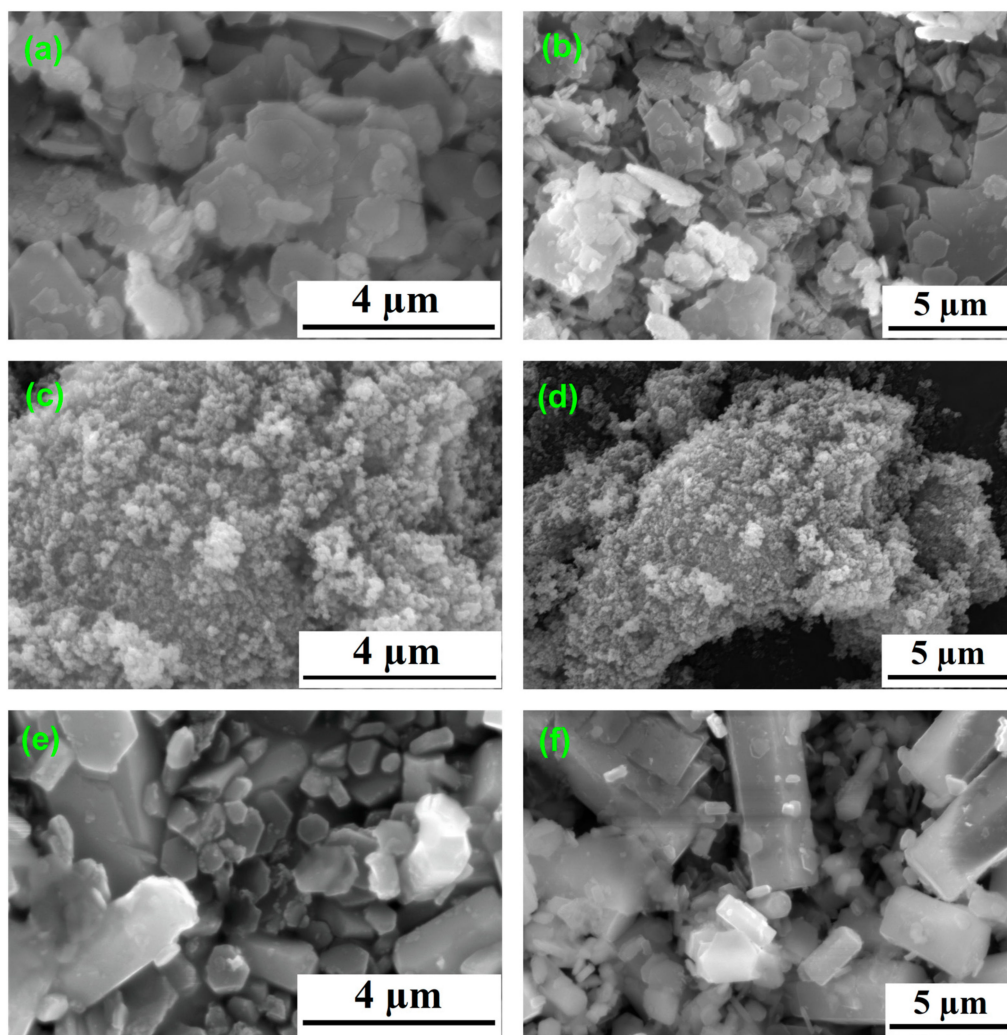
Figure 2. FESEM images to study the morphology, size, and shape of the synthesized ZnO and metal-doped NSs (**a**,**b**) ZnO (**c**,**d**) CuZnO, (**e**,**f**) CoZnO.

The Full Width at Half Maximum (FWHM) measurements was conducted to identify the nanoparticle sizes based on the earlier available data. From the XRD pattern, the mean particle diameter of CuZnO and CoZnO was determined. The size of the nanoparticles was calculated using the Scherer Equation (1).

$$D = \frac{k\lambda}{\beta cos\theta} \tag{1}$$

where average crystallite size is represented by "*D*", *K* represents Scherrer constant, which has a value of 0.94, λ, β & θ represents X-ray wavelength, full width at half maximum, and Braggs angle, respectively. These calculations show that CuZnO has an average particle size of 38.91 nm, while CoZnO has 58.74 nm, i.e., CuZnO has particles of smaller size than CoZnO, these results also confirm the (FE-SEM) results.
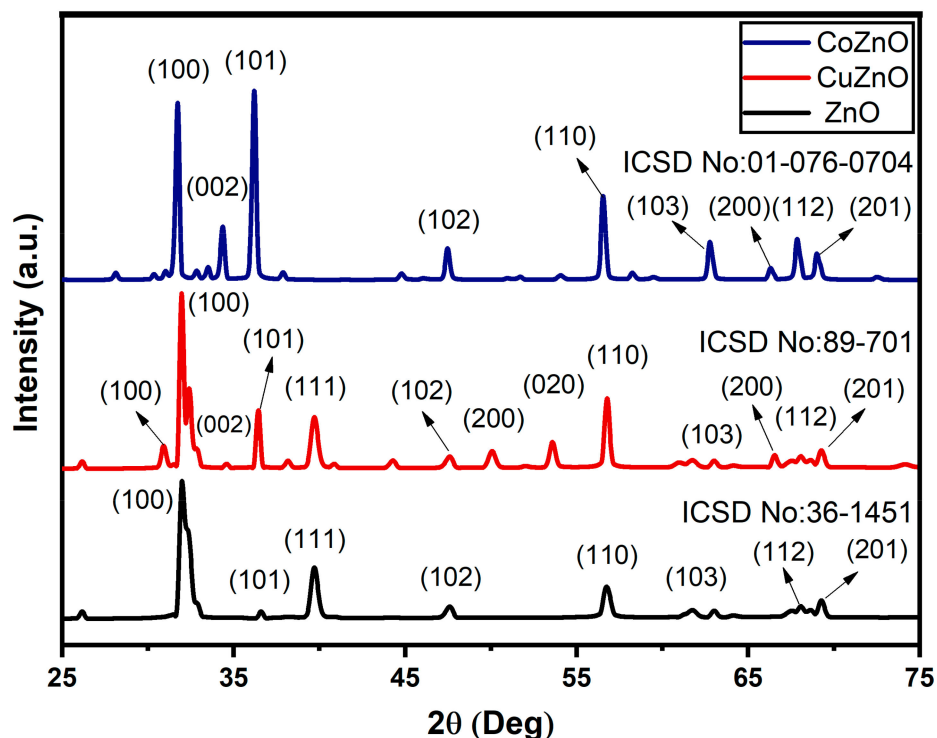
Figure 3. XRD spectrum of ZnO, CuZnO, and CoZnO nanostructures.

3.3. X-ray Photoelectron Spectroscopy

The chemical compositions, valence states, and bonding characteristics of ZnO, CuZnO and CoZnO determined using XPS are shown in Figure 4. Zn 2p, Cu 2p, Co 2p, and O 1s peaks were found and almost no precursor materials or magnetic impurities were detected in the samples. The XPS survey is shown in Figure 4a, and the spots have been identified with the respective binding energies of the individual elements. Along with Zn 2p and O 1s peaks, the survey indicates the high intensities of Cu 2p and Co 2p peaks for Cu and Co contents. In Figure 4b, two noticeable peaks correspond to the spin-orbits of Zn 2p3/2 and Zn 2p1/2 with binding energies of 1022.1 and 1045.2 eV, respectively. A minimal peak shift is noticed while comparing CuZnO and Co ZnO samples which are mostly related to chemical or oxidation states. Figure 4c displays high-resolution Gaussian-fitted XPS scans. The Cu core level splits into Cu $2p_{3/2}$ and Cu $2p_{1/2}$ with binding energies of 934.1 and 954.3 eV. These results are consistent with the hypothesis that Cu appears to be in a bivalent valence state [19]. Another factor connected to the satellite peak noticed in the 940–945 eV band is a cupric oxide (Cu^{2+}) [20]. This demonstrates that Cu ions (Cu^{2+}) were substituted at the Zn^{2+} region in the ZnO crystal after being oxidized in ZnO. Figure 4d displays the Co 2p peaks along with the Co $2p_{3/2}$ peak and Co $2p_{1/2}$ peak, which are respectively located at 780 eV and 796 eV. The incorporation of CO^{2+} is indicated by the binding energy difference (16 eV) observed between the two Co 2p peaks. Thus, the XPS analysis shows that the substitution of Cu^{2+} and Co^{2+} on Zn^{2+} lattice sites is successful with no additional impurities in the ZnO lattice [21]. Additionally, a C 1s signal is found on 285 eV, which may be caused by hydrocarbon contamination possibly due to exposure of the material to air before analysis.
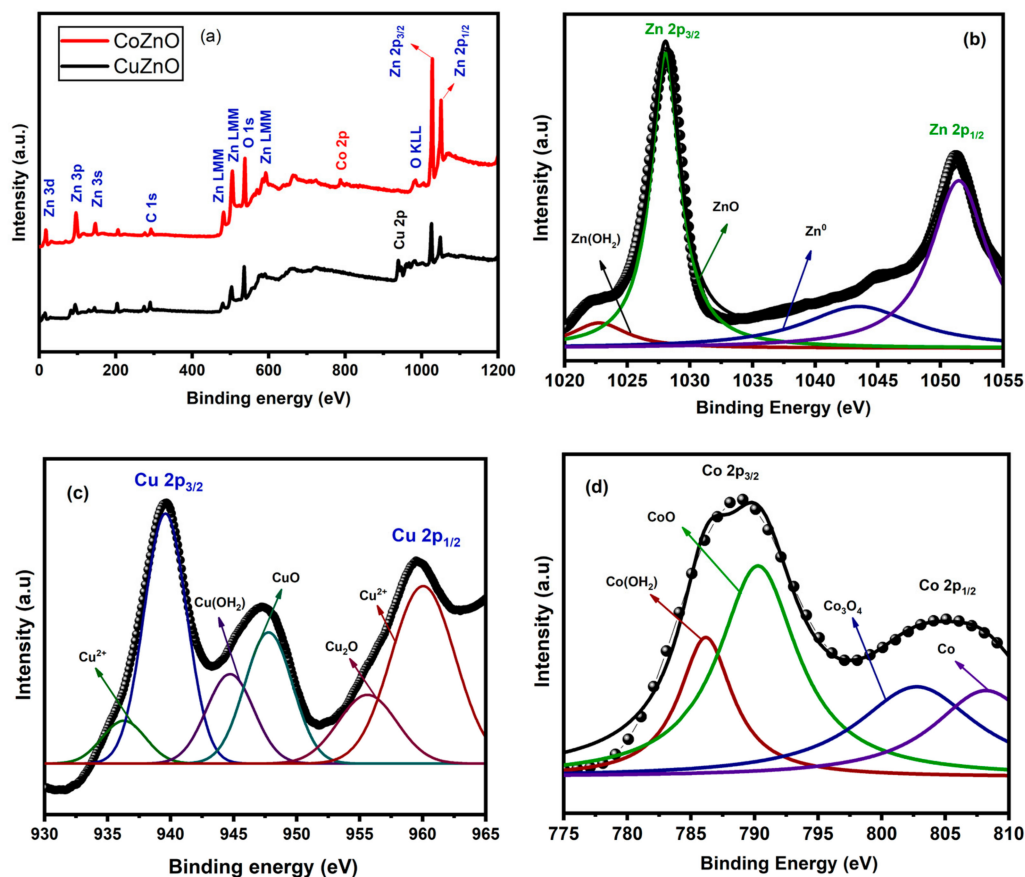
Figure 4. (**a**) XPS survey of CoZnO and CuZnO, (**b**) high-resolution Zn 2p peaks, (**c**) high resolution Cu 2p peaks, and (**d**) high-resolution Cu 2p peaks.

3.4. Raman Spectroscopy

Raman spectroscopic analysis of the synthesized materials was carried out to analyze defects in the structure, lattice disorder, and dopant incorporation in the material. The non-destructive analysis was carried out in the range of 300–600 nm [22]. The as-obtained Raman spectrum for ZnO, CuZnO, and CoZnO as shown in Figure 5 has three main peaks around 355 cm^{-1}, 434 cm^{-1}, and 493 cm^{-1}, respectively. E_2H-E_2L modes, transverse optical (TO) modes, and E_2 (high) modes are responsible for these peaks. The peaks at 350 cm^{-1}, 352 cm^{-1}, and 373 cm^{-1} correspond to the E_2H-E_2L modes of ZnO, CuZnO, and CoZnO, respectively. The peaks at 493 cm^{-1}, 493 cm^{-1}, and 496 cm^{-1} are related to E_2 (high) nonpolar phonon modes of ZnO, CuZnO, and CoZnO, respectively. CuZnO and CoZnO peaks are moved toward higher frequencies in contrast to pure ZnO [23]. The TO mode of vibration is assigned to the high-intensity peaks at 382 cm^{-1}, 382.5 cm^{-1}, and 383 cm^{-1} [24,25]. According to the published literature, the host lattice defects such as Zn interstitials and oxygen vacancies are responsible for the Raman peak at 547 cm^{-1}, and 548 cm^{-1} in the Raman spectrum of the CuZnO and CoZnO. In other terms, this substantially supports the doping of Cu^{2+} and Co^{2+} into the ZnO lattice [24,26].
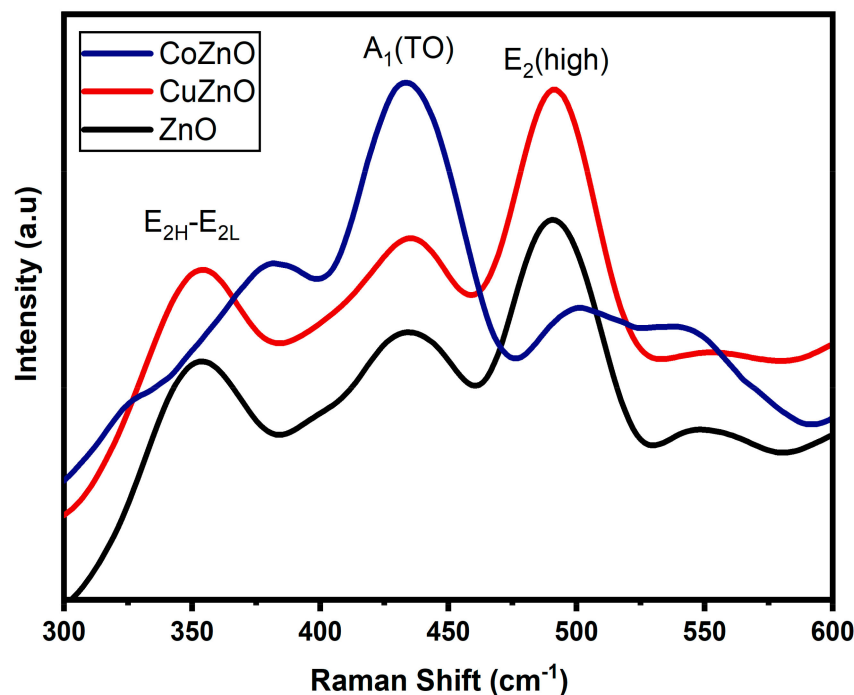
Figure 5. Raman spectrum of the study of ZnO, CuZnO, and CoZnO.

3.5. Photoluminescence Spectroscopy

The optical characteristics of the synthesized materials, including the impact of Cu and Co incorporation in ZnO, were investigated using photoluminescence spectroscopy (PL). The PL spectra of pure and doped materials are shown in Figure 6. The spectrum shows two emission bands for ZnO, including weak (UV) and strong (visible) ranges. Crystal defects and exciton-related transitions could be the potential reasons for strong visible and weak UV emissions [27]. It is confirmed that Co and Cu have a +2 valence state in ZnO. PL spectra were observed in UV and Vis ranges for all analyzed materials. Weak UV bands were observed on 379 nm, 391 nm, and 374 nm in ZnO, CuZnO, and CoZnO respectively, and appeared due to band-to-band exciton transitions. Strong emission bands in the visible range at 537 nm, 569 nm, and 571 nm are formed by the electronic transition in the defect levels for ZnO, CuZnO, and CoZnO band gap. Thus, the relative energy levels and band gap of –sub-band gap defect states can both be investigated using PL spectra. Oxygen vacancies are responsible to produce the green emission at 537 nm, 569 nm, and 571 nm [28]. The broad PL spectra made it impossible to differentiate between the UV and Vis bands.

3.6. Dye Degradation Analysis

The degradation or trimming process of methylene blue (MB) using ZnO, CuZnO, and CoZnO photocatalysts involves the generation of reactive oxygen species (ROS) upon irradiation with light. These ROS, such as hydroxyl radicals ($\bullet OH$), superoxide radicals ($\bullet O_2^-$), and hydrogen peroxide (H_2O_2), can then react with MB molecules and break them down into smaller, less harmful compounds.

In the case of ZnO, the degradation mechanism involves the excitation of electrons from the valence band to the conduction band of ZnO upon absorption of light. These excited electrons can then react with oxygen molecules to form superoxide radicals ($\bullet O_2^-$), which can further react with water to form hydroxyl radicals ($\bullet OH$). The hydroxyl radicals can then react with MB molecules and break them down into smaller compounds.
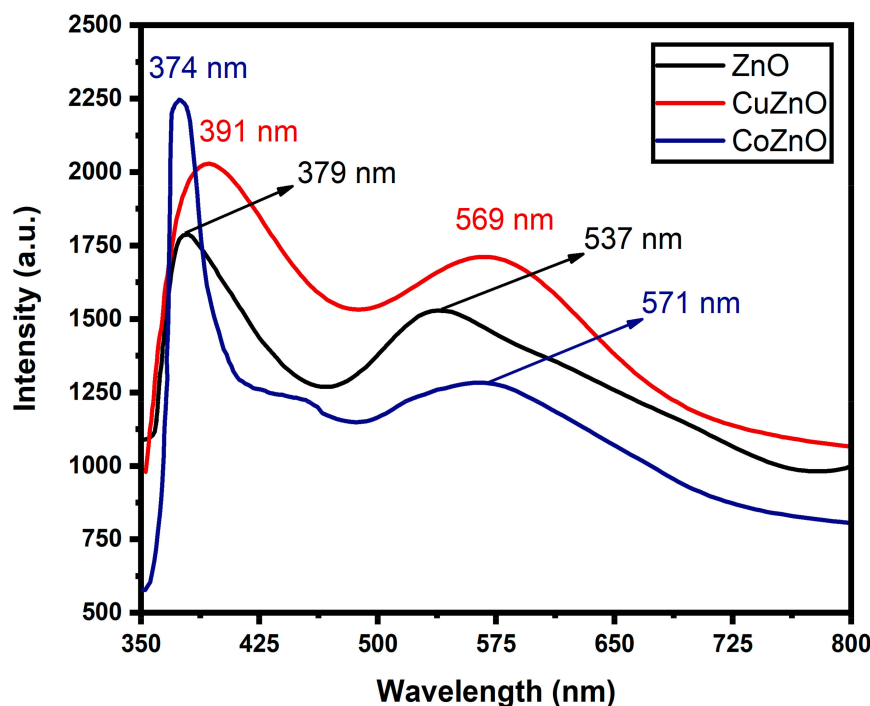
Figure 6. Photoluminescence spectra of ZnO, CoZnO and CuZnO.

For CuZnO and CoZnO photocatalysts, the mechanism is similar, but the presence of Cu or Co can enhance the photocatalytic activity of ZnO. In CuZnO photocatalysts, the Cu dopant can act as an electron trap, increasing the excited electrons' lifetime and improving ROS generation efficiency. Additionally, Cu can also form surface complexes with MB, facilitating its adsorption onto the catalyst surface and increasing the probability of degradation. In CoZnO photocatalysts, the Co dopant can act as a nucleation agent, promoting crystal growth and forming larger particles with higher surface area. This increased surface area can provide more sites for MB adsorption and degradation.

Overall, the degradation or trimming process of MB using ZnO, CuZnO, and CoZnO photocatalysts involves the generation of ROS, which can react with MB molecules and break them down into smaller, less harmful compounds. The presence of dopants such as Cu or Co can enhance the photocatalytic activity of ZnO and improve the efficiency of MB degradation.

3.6.1. Effect of pH

Initially, the effect of pH was checked on the photodegradation of MB dye ranged 2–12 in the presence of a synthesized efficient photocatalyst, with dye concentration = 5 mg/L and catalyst dose = 1 g/L with a contact time of 100 min as illustrated in Figure 7. It can be assumed that for a catalyst, the absorption behavior and surface charge properties are affected by pH of a solution [29]. A substantial increase is observed in dye degradation with an increase in pH value and attains its higher value in the basic pH range (12). As a result, the catalyst surfaces were intensely electrified and became negatively charged at higher pH levels, and the decolorization of MB dye was improved. The highest photodegradation rate (55%, 75%, 90%) is observed on pH~12 while using various pH ranges of ZnO, CoZnO, and CuZnO.
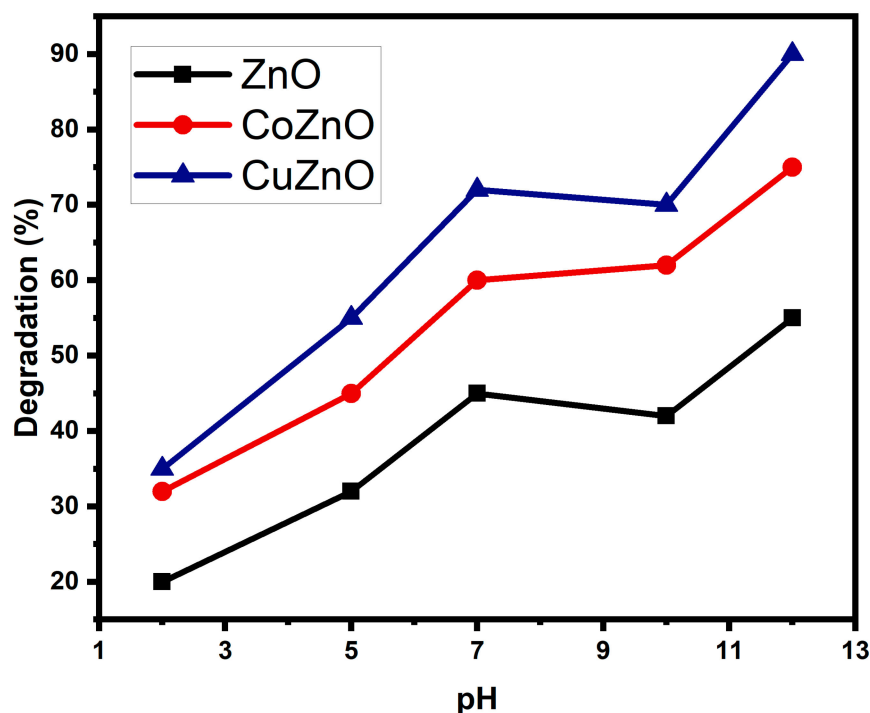
Figure 7. Effect of pH using ZnO, CuZnO, and CoZnO on MB dye.

3.6.2. Effect of Initial Dye Concentration

The catalyst effectiveness was also checked at enhanced pH-12 with different concentrations of methylene blue dye ranging from 5–50 mg/L used to access the photodegradation at the initial concentration of 5 mg/L as clearly shown in Figure 8. The photodegradation rate of dyes decreases with the initial concentration increase. It may be due to the concentration of dyes increasing the access of dyes molecules attached to the surface of the catalyst. The amount of hydroxyl group radicals on the photocatalyst surface will either remain constant for a given irradiation time, light intensity, and catalyst dose or the active sites of the photocatalyst will be lowered as the dye concentration increases [30]. The amount of hydroxyl radicals formed is insufficient to allow the dye to degrade at high concentrations. As a result, photodegradation performance decreases with an increase in dye concentration. Dye degradation is also inversely proportional to MB dye concentration, decreasing from (70% to 22%), (80% to 16%), and (94% to 10%) for ZnO, CoZnO, and CuZnO, respectively as MB concentration is increased from 5 mg/L to 50 mg/L.

3.6.3. Effect of Contact Time

The effect of time on the photodegradation of MB dye was analyzed using a fixed amount of ZnO, CoZnO, and CuZnO catalyst (1 g/L), pH = 12, and 5 mg/L of dye. The relations between the contact time of the photocatalyst and the photodegradation of MB dye were studied as shown in Figure 9. The degradation of MB has been found to increase with increasing catalyst exposure time [31]. The graph shows that the degradation rate initially lowers due to the non-availability of a large number of active sites, and repulsion between the catalyst surface and dye particles. Degradation of the dyes is related to irradiation duration, with 60%, 70%, and 89% of the MB dye being destroyed using ZnO, CoZnO and CuZnO in 100 min.
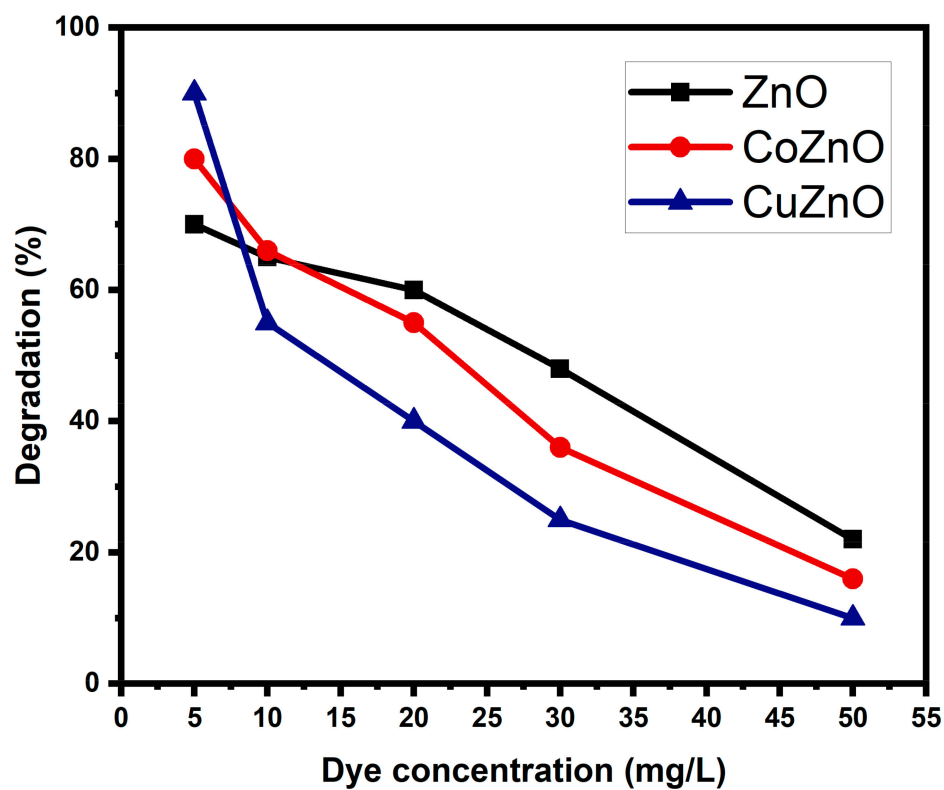
Figure 8. Effect of dye concentration on the dye degradation behavior of photocatalysts.
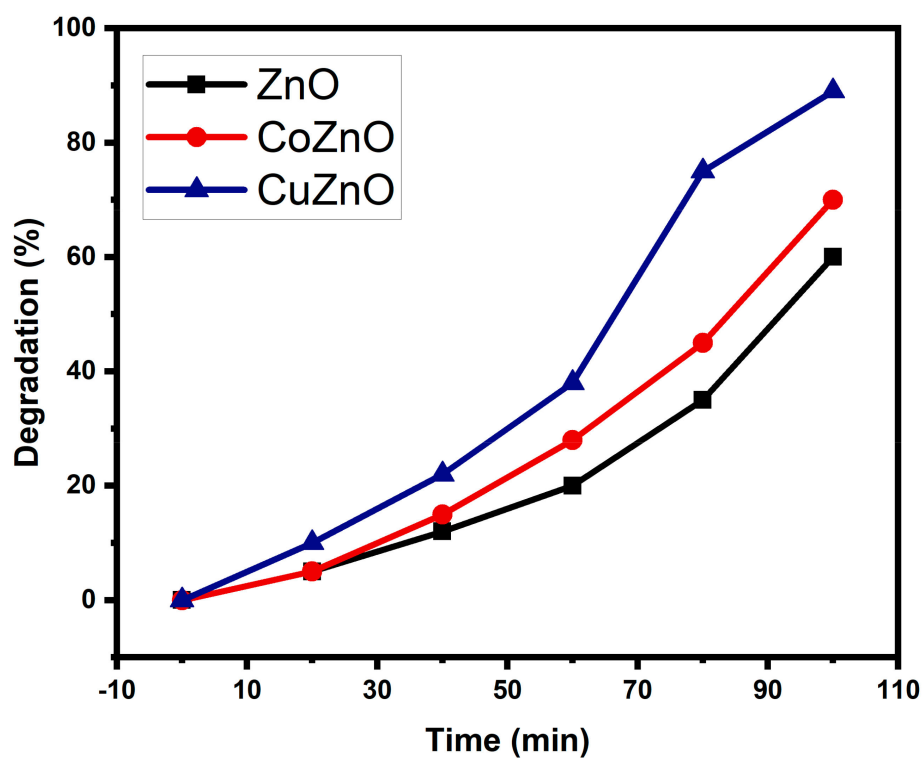

Figure 9. Effect of time on the dye degradation behavior of ZnO, CuZnO, and CoZnO.

3.6.4. Effect of Catalyst Dose

The degradation percentage was also checked at different amounts of catalyst by keeping other experimental condition constant (pH = 12, dye concentration 5 mg/L, and contact time 100 min). The photodegradation was carried out by various doses of the catalyst (0.1–1 g/L). Figure 10 explicitly states that the particle-to-particle interface improves as catalyst concentration rises, and this is the main factor limiting photocatalysts absorbing light. Additionally, photons are unable to penetrate the catalyst's inner layers due to the agglomerations [32]. As a result, fewer catalyst particles are stimulated, which results in a lower number of electrons/holes and hydroxyl radicals being formed. Therefore. the rate of degradation tends to slow down as the catalyst dose rises [33]. Direct variation is observed in catalyst concentration analysis as 60%, 70%, and 89% dye degraded for ZnO, CoZnO, and CuZnO using a 1 g photocatalyst.
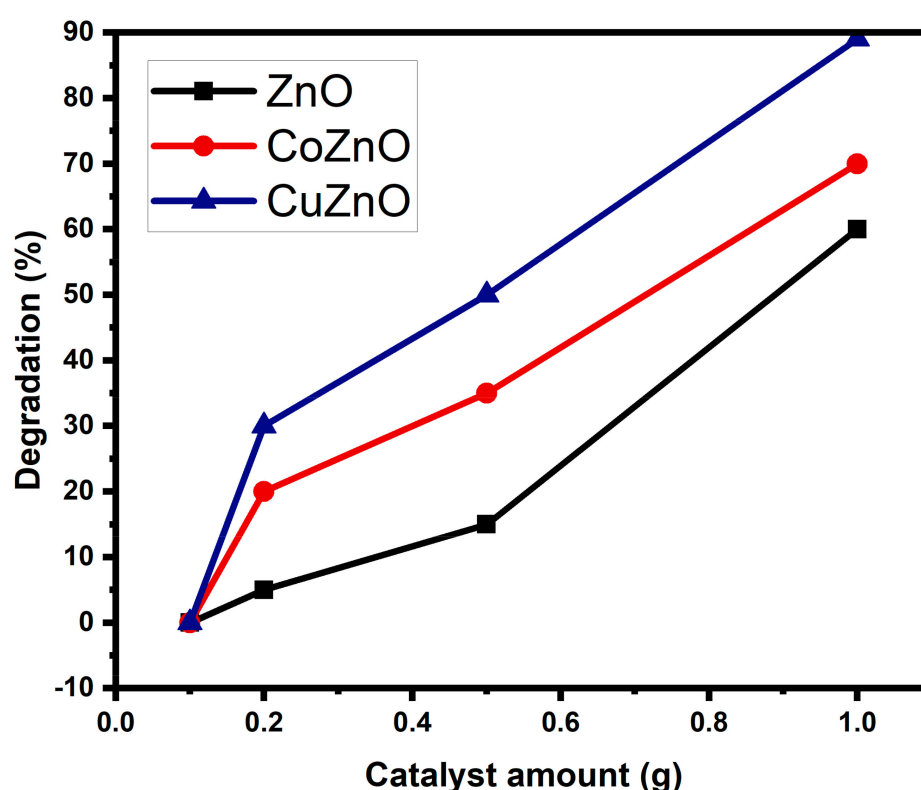

Figure 10. Effect of photocatalyst amount on MB dye degradation.

Photodegradation behavior of MB dye when exposed for 100 min using ZnO, CoZnO and CuZnO photocatalysts is shown in Figure 11. The study further determined the optimal nanocatalyst recyclability for the photodegradation of MB dye. After five consecutive photodegradation tests employing the same catalyst, the metal oxide nanocatalyst demonstrated adequate stability; however, the photodegradation yield decreased by 45% and 15% after the first and fifth cycles. After five cycles, recycling studies reveal that photostability is retained following the doping process, indicating that CuZnO and CoZnO are effective as recyclable photocatalysts for sunlight-driven photodegradation.
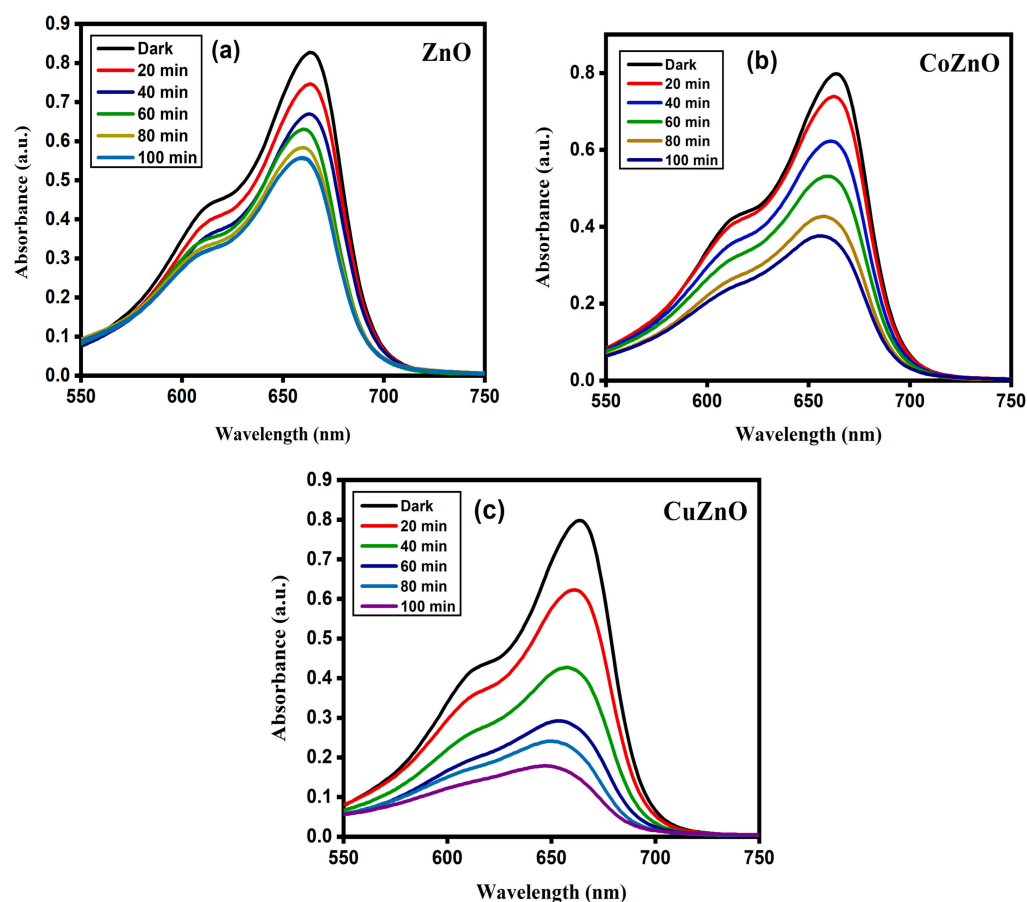
Figure 11. Complete photodegradation behavior of MB dye in 100 min using (**a**) ZnO, (**b**) CoZnO, and (**c**) CuZnO photocatalysts.

4. Conclusions

In this study morphological, structural, and spectroscopic analysis of ZnO, CuZnO, and CoZnO is presented in detail. XPS indicates that Co and Cu were incorporated inside ZnO after doping. Besides, the photocatalysis test indicated that degradation of the dyes is related to irradiation duration, with 60%, 70%, and 89% of the MB dye being destroyed using ZnO, CoZnO, and CuZnO in 100 min. Direct variation is observed in catalyst concentration analysis as 60%, 70%, and 89% dye degraded for ZnO, CoZnO and CuZnO using 1 g photocatalyst. Dye degradation is also inversely proportional to MB dye concentration, decreasing from (70% to 22%), (80% to 16%), and (94% to 10%) for ZnO, CoZnO and CuZnO, respectively as MB concentration is increased from 5 mg/L to 50 mg/L. The highest photodegradation rate (55%, 75%, 90%) is observed on pH~12 while using various pH ranges of ZnO, CoZnO and CuZnO. Finally, the photodegradation percentage for CuZnO is higher than that for CoZnO and pure ZnO. As a result of enhanced photodegradation efficiency against MB dye, CuZnO can be used in wastewater treatment materials.

Author Contributions: Conceptualization, A.K., P.A., M.U.K. and H.A.A.; methodology, Y.M., R.M. and L.F.G.; formal analysis, A.K.; investigation, A.K. and P.A.; resources, Y.M., F.A.A., O.A., A.T. and H.A.A.; writing—original draft preparation, A.K., R.M., L.F.G., Y.M. and N.B.; writing—review and editing, A.K., P.A., R.M., L.F.G., M.U.K., H.A.A., A.T., O.A., F.A.A. and Y.M.; visualization, A.K., F.A.A. and N.B.; project administration, A.K., P.A. and M.U.K.; funding acquisition, A.K., A.T., O.A. and M.U.K. All authors have read and agreed to the published version of the manuscript.

Data Availability Statement: All the data are available in the manuscript.

Conflicts of Interest: The authors declare no conflict of interest.

References

1. Kumaresan, N.; Ramamurthi, K.; Babu, R.R.; Sethuraman, K.; Babu, S.M. Hydrothermally grown ZnO nanoparticles for effective photocatalytic activity. *Appl. Surf. Sci.* **2017**, *418*, 138–146. [CrossRef]
2. Zhu, L.; Li, H.; Liu, Z.; Xia, P.; Xie, Y.; Xiong, D. Synthesis of the 0D/3D CuO/ZnO Heterojunction with Enhanced Photocatalytic Activity. *J. Phys. Chem. C* **2018**, *122*, 9531–9539. [CrossRef]
3. Hafeez, M.; Afyaz, S.; Khalid, A.; Ahmad, P.; Khandaker, M.U.; Sahibzada, M.U.K.; Ahmad, I.; Khan, J.; Alhumaydhi, F.A.; Bin Emran, T.; et al. Synthesis of cobalt and sulphur doped titanium dioxide photocatalysts for environmental applications. *J. King Saud Univ.-Sci.* **2022**, *34*, 102028. [CrossRef]
4. Khalid, A.; Ahmad, P.; Alharthi, A.I.; Muhammad, S.; Khandaker, M.U.; Faruque, M.R.I.; Din, I.U.; Alotaibi, M.A. A practical method for incorporation of Fe (III) in Titania matrix for photocatalytic applications. *Mater. Res. Express* **2021**, *8*, 045006. [CrossRef]
5. Khalid, A.; Ahmad, P.; Khan, A.; Khandaker, M.U.; Kebaili, I.; Alam, M.; Din, I.U.; Muhammad, S.; Razzaq, Z.; Rehman, I.U.; et al. Cytotoxic and photocatalytic studies of hexagonal boron nitride nanotubes: A potential candidate for wastewater and air treatment. *RSC Adv.* **2022**, *12*, 6592–6600. [CrossRef] [PubMed]
6. Khalid, A.; Ahmad, P.; Muhammad, S.; Khan, A.; Khandaker, M.U.; Alam, M.; Asim, M.; Din, I.U.; Iqbal, J.; Rehman, I.U.; et al. Synthesis of Boron-Doped Zinc Oxide Nanosheets by Using Phyllanthus Emblica Leaf Extract: A Sustainable Environmental Applications. *Front. Chem.* **2022**, *10*, 930620. [CrossRef]
7. Razzaq, Z.; Khalid, A.; Ahmad, P.; Farooq, M.; Khandaker, M.; Sulieman, A.; Rehman, I.; Shakeel, S.; Khan, A. Photocatalytic and Antibacterial Potency of Titanium Dioxide Nanoparticles: A Cost-Effective and Environmentally Friendly Media for Treatment of Air and Wastewater. *Catalysts* **2021**, *11*, 709. [CrossRef]
8. Shakeel, S.; Talpur, F.N.; Sirajuddin; Anwar, N.; Iqbal, M.A.; Ibrahim, A.; Afridi, H.I.; Unar, A.; Khalid, A.; Ahmed, I.A.; et al. Xanthan Gum-Mediated Silver Nanoparticles for Ultrasensitive Electrochemical Detection of Hg^{2+} Ions from Water. *Catalysts* **2023**, *13*, 208. [CrossRef]
9. Khalid, A.; Ahmad, P.; Khan, A.; Muhammad, S.; Khandaker, M.U.; Alam, M.; Asim, M.; Din, I.U.; Chaudhary, R.G.; Kumar, D.; et al. Effect of Cu Doping on ZnO Nanoparticles as a Photocatalyst for the Removal of Organic Wastewater. *Bioinorg. Chem. Appl.* **2022**, *2022*, 1–12. [CrossRef]
10. Timoumi, A.; Wederni, M.; Bouguila, N.; Jamoussi, B.; AL Turkestani, M.; Chakroun, R.; Al-Mur, B. Electrical impedance spectroscopy study of unsubstituted palladium (II) phthalocyanine. *Synth. Met.* **2020**, *272*, 116659. [CrossRef]
11. Lu, Y.; Lin, Y.; Wang, D.; Wang, L.; Xie, T.; Jiang, T. A high performance cobalt-doped ZnO visible light photocatalyst and its photogenerated charge transfer properties. *Nano Res.* **2011**, *4*, 1144–1152. [CrossRef]
12. Kuriakose, S.; Satpati, B.; Mohapatra, S. Enhanced photocatalytic activity of Co doped ZnO nanodisks and nanorods prepared by a facile wet chemical method. *Phys. Chem. Chem. Phys.* **2014**, *16*, 12741–12749. [CrossRef] [PubMed]
13. Goswami, M. Enhancement of photocatalytic activity of synthesized Cobalt doped Zinc Oxide nanoparticles under visible light irradiation. *Opt. Mater.* **2020**, *109*, 110400. [CrossRef]
14. Wojnarowicz, J.; Kusnieruk, S.; Chudoba, T.; Gierlotka, S.; Lojkowski, W.; Knoff, W.; Lukasiewicz, M.I.; Witkowski, B.S.; Wolska, A.; Klepka, M.T.; et al. Paramagnetism of cobalt-doped ZnO nanoparticles obtained by microwave solvothermal synthesis. *Beilstein J. Nanotechnol.* **2015**, *6*, 1957–1969. [CrossRef] [PubMed]
15. Ahmad, P.; Khalid, A.; Khandaker, M.U.; Rehman, F.; Khan, M.I.; Ali, H.; Muhammad, N.; Kiyani, M.S.; Sulieman, A.; Razzaq, Z.; et al. The antibacterial and antioxidant efficacy and neutron sensing potency of 10B enriched hexagonal boron nitride nanoparticles. *Mater. Sci. Semicond. Process.* **2021**, *141*, 106419. [CrossRef]
16. Ganesh, R.S.; Durgadevi, E.; Navaneethan, M.; Patil, V.; Ponnusamy, S.; Muthamizhchelvan, C.; Kawasaki, S.; Patil, P.; Hayakawa, Y. Tuning the selectivity of NH3 gas sensing response using Cu-doped ZnO nanostructures. *Sensors Actuators A Phys.* **2017**, *269*, 331–341. [CrossRef]
17. Kanmani, S.S.; Ramachandran, K. Role of aqueous ammonia on the growth of ZnO nanostructures and its influence on solid-state dye sensitized solar cells. *J. Mater. Sci.* **2012**, *48*, 2076–2091. [CrossRef]
18. Basit, R.A.; Abbasi, Z.; Hafeez, M.; Ahmad, P.; Khan, J.; Khandaker, M.U.; Al-Mugren, K.S.; Khalid, A. Successive Photocatalytic Degradation of Methylene Blue by ZnO, CuO and ZnO/CuO Synthesized from *Coriandrum sativum* Plant Extract via Green Synthesis Technique. *Crystals* **2023**, *13*, 281. [CrossRef]
19. Mosselmans, J.F.; Pattrick, R.A.; Van der Laan, G.; Charnock, J.M.; Vaughan, D.J.; Henderson, C.M.; Garner, C.D. X-ray absorption near-edge spectra of transition metal disulfides FeS₂ (pyrite and marcasite), CoS₂, NiS₂ and CuS₂, and their isomorphs FeAsS and CoAsS. *Phys. Chem. Miner.* **1995**, *22*, 311–317. [CrossRef]
20. Meda, L.; Cerofolini, G.F. A decomposition procedure for the determination of copper oxidation states in Cu-zeolites by XPS. *Surf. Interface Anal.* **2004**, *36*, 756–759. [CrossRef]
21. Narasimman, S.; Balakrishnan, L.; Alex, Z.C. Fiber optic magnetic field sensor using Co doped ZnO nanorods as cladding. *RSC Adv.* **2018**, *8*, 18243–18251. [CrossRef] [PubMed]

22. Singhal, A.; Achary, S.N.; Manjanna, J.; Chatterjee, S.; Ayyub, P.; Tyagi, A.K. Chemical Synthesis and Structural and Magnetic Properties of Dispersible Cobalt- and Nickel-Doped ZnO Nanocrystals. *J. Phys. Chem. C* **2010**, *114*, 3422–3430. [CrossRef]

23. Taher, F.A.; Abdeltwab, E. Shape-controlled synthesis of nanostructured Co-doped ZnO thin films and their magnetic properties. *Crystengcomm* **2018**, *20*, 5844–5856. [CrossRef]

24. Pal, B.; Giri, P.K. High temperature ferromagnetism and optical properties of Co doped ZnO nanoparticles. *J. Appl. Phys.* **2010**, *108*, 084322. [CrossRef]

25. Irshad, M.I.; Ahmad, P.; Khalid, A.; Alam, M.; Sobahi, N.; Din, I.U.; Nazir, R.; Alharthi, A.I.; Rehman, F.; Yar, A.; et al. Evaluation of structural, magnetic and concentration dependent texture variations of electrodeposited cobalt nanowires. *Mater. Sci. Semicond. Process.* **2022**, *152*, 107042. [CrossRef]

26. Duan, L.B.; Rao, G.H.; Wang, Y.C.; Yu, J.; Wang, T. Magnetization and Raman scattering studies of (Co, Mn) codoped ZnO nanoparticles. *J. Appl. Phys.* **2008**, *104*, 013909. [CrossRef]

27. Ansari, S.A.; Khan, M.M.; Kalathil, S.; Nisar, A.; Lee, J.; Cho, M.H. Oxygen vacancy induced band gap narrowing of ZnO nanostructures by an electrochemically active biofilm. *Nanoscale* **2013**, *5*, 9238–9246. [CrossRef]

28. Hameed, A.S.H.; Karthikeyan, C.; Sasikumar, S.; Kumar, V.S.; Kumaresan, S.; Ravi, G. Impact of alkaline metal ions Mg^{2+}, Ca^{2+}, Sr^{2+} and Ba^{2+} on the structural, optical, thermal and antibacterial properties of ZnO nanoparticles prepared by the co-precipitation method. *J. Mater. Chem. B* **2013**, *1*, 5950–5962. [CrossRef]

29. Fatehah, M.O.; Aziz, H.A.; Stoll, S. Stability of ZnO nanoparticles in solution. Influence of pH, dissolution, aggregation and disaggregation effects. *J. Colloid Sci. Biotechnol.* **2014**, *3*, 75–84. [CrossRef]

30. Marathe, Y.V.; Ramanna, M.; Shrivastava, V. Synthesis and characterization of nanocrystalline CdS thin films grown by chemical bath deposition at different molarities for removal of methylene blue. *Desalination Water Treat.* **2013**, *51*, 5813–5820. [CrossRef]

31. Farzi, G.; Tayebee, R.; Naghibinasab, S. *Surface Modification of ZnO Nano-Particles with Trimetoxyvinyl Silane and Oleic Acid and Studying Their Dispersion in Organic Media*; Islamic Azad University: Tonekabon Branch, Iran, 2015.

32. Ajoudanian, N.; Nezamzadeh-Ejhieh, A. Enhanced photocatalytic activity of nickel oxide supported on clinoptilolite nanoparticles for the photodegradation of aqueous cephalexin. *Mater. Sci. Semicond. Process.* **2015**, *36*, 162–169. [CrossRef]

33. Jaffer Sadiq, M.M.; Samson Nesaraj, A. Reflux condensation synthesis and characterization of Co_3O_4 nanoparticles for photocatalytic applications. *Iran. J. Catal.* **2014**, *4*, 219–226.